Optimization of a Flywheel PMSM with an External Rotor and a Slotless Stator

S.R Holm*, H. Polinder** and J.A. Ferreira**

Abstract - An electrical machine for a high-speed flywheel for energy storage in large hybrid electric vehicles is described. Design choices for the machine are motivated: it is a radial-flux external-rotor permanent-magnet synchronous machine without slots in the stator iron and with a shielding cylinder. An analytical model of the machine is briefly introduced whereafter optimization of the machine is discussed. Three optimization criteria were chosen: (1) torque; (2) total stator losses and (3) induced eddy current loss on the rotor. The influence of the following optimization variables on these criteria is investigated: (1) permanent-magnet array; (2) winding distribution and (3) machine geometry. The paper shows that an analytical model of the machine is very useful in optimization.

Keywords: hybrid electric vehicle, permanent-magnet synchronous machine(PMSM), permanent magnet array, flywheel, eddy current loss

1. Introduction

Hybrid electric vehicles require a much lower specific energy [J/kg] from their electrical energy storage technology than pure electric vehicles [1], [2]. A high specific power [W/kg] of the energy storage technology is, however, crucial in hybrids. Careful design to minimize the overall storage losses in the energy storage system is therefore required, since higher losses lead to a lower specific power. In optimizing such an energy storage system, the following optimization criteria are therefore chosen: maximum power and minimum losses.

It is beyond the scope of this paper to compare energy storage technologies in an attempt to find the most suitable one for use in a hybrid electric vehicle. (Such a comparison is extensively done in [2].) In summary, composite flywheel energy storage systems are well-suited to high-power applications (more than approximately 100 kW) where a high specific power is more important than a high specific energy. From the discussion above, this is exactly what is required by hybrid electric vehicles. A composite flywheel system is therefore chosen for use in a new hybrid electric bus project (Phileas) launched in the city of Eindhoven, the Netherlands (see Fig. 1).

Fig. 2 shows a typical electrical system of such a hybrid electric bus. The primary energy source is LPG, converted to mechanical energy by the internal combustion engine (ICE) and then to electrical energy (dc) by an ac generator with rectifier. This dc bus forms the heart of the system. Electrical power is drawn through a frequency converter (VSI) from this bus by the traction machine and delivered to the driving wheels. The flywheel machine draws power from the dc bus through a current-source inverter (CSI) during charging. Power can also be delivered to the dc bus by the flywheel machine during discharging and by the traction machine during regenerative braking. This regenerated energy can then be redirected into the flywheel to charge it up again.

Fig. 1 A newly developed hybrid electric city bus, Phileas, recently introduced into the public transport system in Eindhoven, the Netherlands.

In a system as in Fig. 2, the primary power source (the ICE) only needs to be dimensioned for the average power demand of the load. The peak power demand (during acceleration from standstill or driving up a steep hill, for example) is delivered by the secondary power source, the flywheel system.

The rest of the paper is concerned only with the electrical machine integrated into the flywheel. More specifically, the optimization of the machine with respect to the two chosen criteria (high power and low losses) is discussed.

2. Electrical machine design choices

The first choice is which type and geometry of machine to use for this application. Concerning the machine type, a permanent-magnet machine is chosen because of its high torque density.

* University of Johannesburg, Johannesburg, South Africa. (robertholm@ieee.org)

** Delft University of Technology, Delft, the Netherlands.

Received April 19, 2005 ; Accepted August 23, 2005

Choosing between radial and axial flux machine topologies is done by investigating flywheel theory as in [3], [4]. A composite (carbon fibre / fibre glass) flywheel cannot be made solid since the forces on the material require isotropic strength properties (composite materials are higly anisotropic). A rimmed flywheel is therefore obtained, i.e., there is a large "hole" in the center of the flywheel. Since the object of the design is to achieve as high a specific power as possible, no material or space is to be wasted.

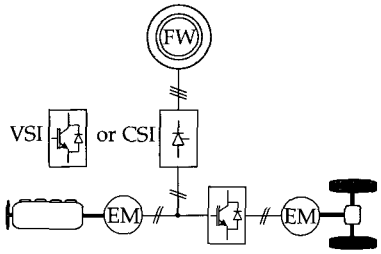

Fig. 2 The electrical system of the hybrid electric bus. (Nomenclature: "FW" = flywheel; "VSI" = voltage-source inverter; "CSI" = current-source inverter; and "EM" = electrical machine.)

Therefore it makes sense to integrate the electrical machine into the flywheel; the logical location to place the machine is in the center hole. This leaves the only feasible topology to be an external-rotor radial flux one, with the permanent magnets and rotor yoke fixed to the flywheel itself. This construction is also feasible for magnet containment since the rotational forces press the magnets harder into the flywheel in stead of trying to rip them off as is the case in an internal rotor.

A predecessor of the electrical machine developed for this project exhibited quite substantial no-load losses. These were mainly concentrated in the stator iron teeth [4]. A natural solution to this problem is to remove the stator teeth --- the stator then becomes slotless. The main disadvantages of this approach are that the air gap flux density decreases and that the stator conductors are directly inside the magnetic field, leading to eddy-current loss. However, in a study done by Arkadan, Vyas, Vaidya and Sha [5], it is shown that by appropriate design of a Litz wire winding, the eddy-current loss disadvantage is almost completely eliminated while also drastically reducing the stator iron losses. The reduction in air gap flux density has to be solved by using thickerpermanent magnets. For the machine under discussion in this paper, therefore, a slotless stator is used. Furthermore, the stator winding is chosen to be distributed as commonly used in synchronous machine stators to approach a sinusoidal winding distribution. (Opposed to the concentrated windings of brushless dc machines.)

In [6], [7], [8], [9], [10] and [11], among others, the effect of a shielding cylinder on the rotor losses in permanent-magnet machines has been investigated. This cylinder shields the permanent magnets and the rotor iron from high-frequency magnetic fields originating from the stator currents. One general conclusion was that for low rotational speeds, the addition of a shielding cylinder increases the losses while for high rotational speeds, the losses are reduced by the addition of a shielding cylinder. In [10], it is furthermore recommended that in the case where solid rotor iron is used, a shielding cylinder should always be used to reduce the rotor losses. Since the flywheel machine requires a solid rotor iron yoke for mechanical reasons, a shielding cylinder is used in the machine.

In summary, the electrical machine is a radial-flux external-rotor permanent-magnet synchronous machine without slots in the stator iron and with a shielding cylinder. Fig. 3 shows a radial cross section of the machine.

3. Analytical model

An analytical model of the machine was derived. The motivation for using an analytical model as opposed to a finite-element approach is based on these two facts: (1) the machine geometry of Fig. 3 is ideally suited to an analytical approach and (2) an analytical approach leads to greater insight into the problem. For an extensive discussion of the analytical model used in this optimization study, see [2].

4. Optimization

4.1 Optimization criteria

The optimization criteria of high power and low losses have already been stated in Sec. I. The "low losses" criterion is now expanded to mean: "very low rotor losses" and "low stator losses."

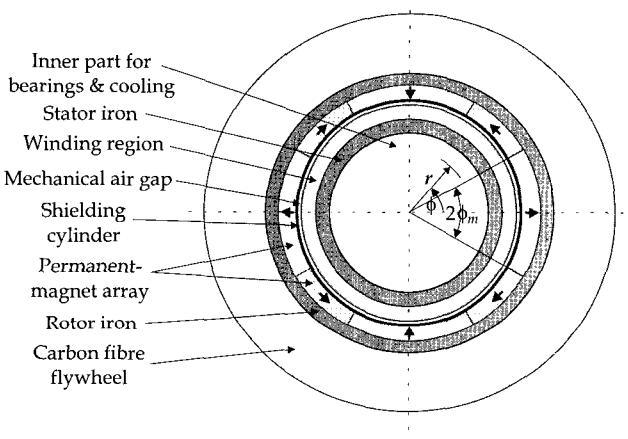

Fig. 3 A radial cross section of the flywheel machine geometry. The permanent-magnet array is shown to be a discrete Halbach array with two segments per pole (for example).

The reason for very low rotor losses is that since the rotor rotates at very high speed in a low-pressure atmosphere, it is extremely difficult to cool. Furthermore, a too high rotor temperature will lead to demagnetization of the magnets.

The criterion "high power" translates to "high torque" at a given rotational speed.

4.2 Optimization variables

The optimization variables chosen for the optimization procedure were: (1) permanent-magnet array; (2) winding distribution; (3) machine geometry. Several other variables may be identified but these three were chosen as the most important.

4.3 Permanent-magnet array

By permanent-magnet array is meant the configuration of the permanent magnets (only surface-mounted arrays are considered here). For example, a radial array has only radially magnetized magnets with an inter-magnet spacing (air) that fills 20\% of the circumference. Another way to see a radial array is that it is a discrete Halbach array with one segment per pole (see [12], [13] for a description of Halbach arrays). Different permanent-magnet arrays may be described by the number of segments per pole, the pole arc variation and the number of pole pairs.

1) *The number of segments per pole:* Three different arrays with a different number of segments per pole were investigated for this paper. These are: the radial array ($n_{seg} = 1$), the discrete Halbach array with 2 segments per pole ($n_{seg} = 2$) and the ideal Halbach array ($n_{seg} \rightarrow \infty$). (The ideal Halbach array is effectively obtained in the limit when the number of segments per pole reaches infinity.)
2) *Pole arc variation and the number of pole pairs:* In the investigation of the influence of the optimization variables on the optimization criteria, pole arc variation was also studied. In other words, the customarily used polar magnet arc of 80% per pole for the radial array was not used but the variation thereof was studied. Similarly, the 50/50 distribution between the space taken up by the radially and tangentially magnetized magnets was not used in the discrete Halbach array with $n_{seg} = 2$, but its variation was investigated.

The influence of varying the number of pole pairs p on the optimization criteria was also investigated.

4.4 Winding distribution

In the flywheel machine, the stator winding distribution was required to have a low space harmonic content, i.e., to closely approximate a sinusoidal winding distribution. The main reason for this is to limit the eddy-current loss induced in the shielding cylinder. The winding has more than one layer (the number depends on which distribution is used) and is in fact constructed as a slotted structure, but the slots are made of a synthetic nonmetallic material. See Fig. 4 for a picture of the slotless winding during the winding process.

The influence of the four different winding distributions shown in Fig. 5, on the optimization criteria were investigated. Two of these utilize short pitching (the 1-2-2-1 and the 1-1-2-1-1 distributions) and the other two do not (the 2-2-2 and the 3-3 distributions).

4.5 Machine geometry

By machine geometry is meant the relationship of the various radii in the machine with respect to each other. The changes in the electromagnetic torque (T_e) production and the losses by varying these machine radii are studied.

See Fig. 6 for the radii that are varied in the optimization procedure and those that stay constant. In Fig. 6, r_{si} is the stator inside radius, r_{so} the stator outside radius, r_w the winding outside radius, r_{ci} the shielding cylinder inside radius, r_{co} the shielding cylinder outside radius, r_{mi} the magnet array inside radius, r_{mo} the magnet array outside radius, and r_{mo} the rotor iron outside radius.

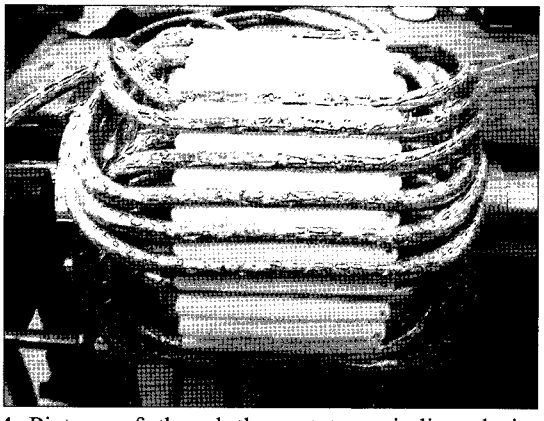

Fig. 4 Picture of the slotless stator winding during the winding process.

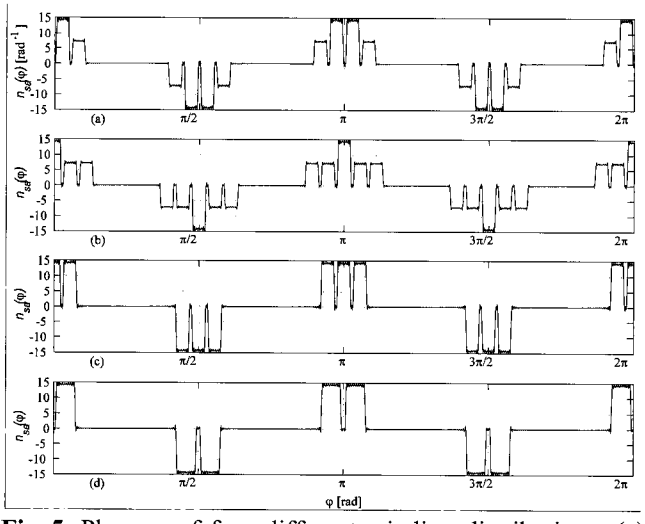

Fig. 5 Phase a of four different winding distributions: (a) 1-2-2-1; (b) 1-1-2-1-1; (c) 2-2-2 and (d) 3-3.

Fixed r_{so} and r_{mo} were first considered (obtained from a mechanical design iteration of the flywheel done by CCM). The three radii in between, r_w, r_{ci} and $r_{co} = r_{mi}$, are varied with a constant ratio to each other. In other words, the magnet inner radius r_{mi} is varied with respect to r_{so} and r_{mo}, and while doing this, the distance between r_{mi}, r_{ci} and r_w remains constant. Therefore, a constant mechanical air gap r_{ci} - r_w is assumed, and also a constant shielding cylinder thickness r_{co} - r_{ci}.

A ratio between the magnet thickness and the total distance between the stator and rotor surfaces can be defined:

$$R_m = (r_{mo} - r_{mi})/(r_{mo} - r_{so}). \quad (1)$$

As R_m is varied, its influence on T_e and the losses is investigated.

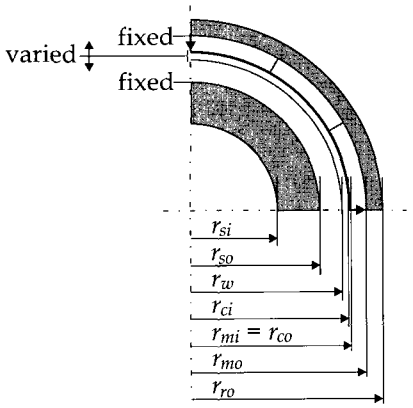

Fig. 6 Definition of the radii that are varied and those that stay constant in a study of electromagnetic torque and losses as a function of the machine geometry.

5. Optimization results

5.1 Permanent-magnet array

The influence of the pole arc and the number of pole pairs on the fundamental component of the electromagnetic torque and the stator iron losses is presented in this section. The rotor losses are not influenced by the permanent-magnet array.

5.1.1 Electromagnetic torque

Fig. 7 shows the variation in the fundamental space and time harmonic component of T_e with polar magnet span. The results for two-, four- and eight-pole machines are shown in Fig. 7(a), (b) and (c), respectively. Each graph shows the results for the three permanent-magnet arrays under discussion in this paper. It can be seen from Fig. 7(a), (b) and (c) that:

- The difference between the radial array and the discrete Halbach array is larger for a larger number of pole pairs.
- The polar arc for which the torque produced by the discrete Halbach array equals that of the ideal Halbach array is approximately 60% for all p resented. The difference in this breakeven torque for the radial array is higher as p increases.
- The peak torque for the radial and discrete Halbach arrays drops with increasing p, this is due to the reduced coupling and thus larger leakage field for higher p (the geometry stays constant).

5.1.2 Stator iron losses

Fig. 8 shows the total losses induced in the stator iron as a function of the polar magnet span and the number of pole pairs: (a) $p = 1$; (b) $p = 2$ and (c) $p = 4$. The calculation was done for the first 13 space harmonics.

As for the torque, the difference between the radial array and the discrete Halbach array is larger for a larger number of pole pairs. Also, the induced stator losses are drastically less for higher p due to the lower flux density in the iron.

5.2 Winding distribution

5.2.1 Electromagnetic torque

The fundamental space and time harmonic of the electromagnetic torque for the four different winding

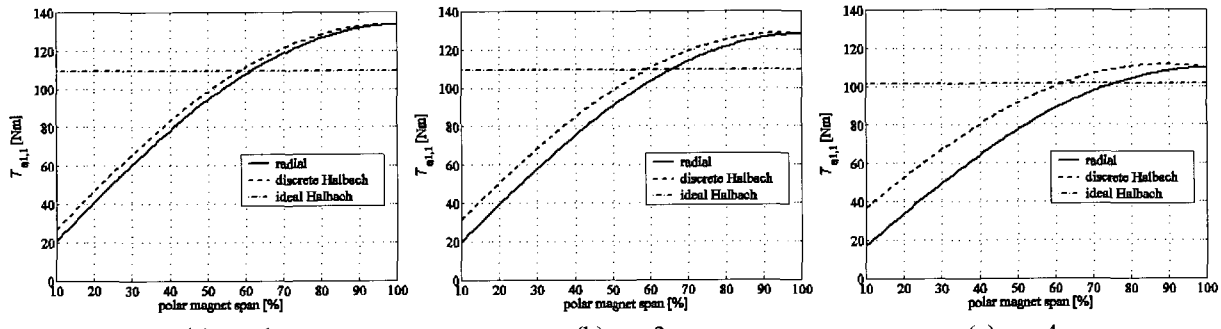

(a) $p = 1$ (b) $p = 2$ (c) $p = 4$

Fig. 7 Fundamental space and time harmonic component of the torque as a function of the polar magnet span and the number of pole pairs.

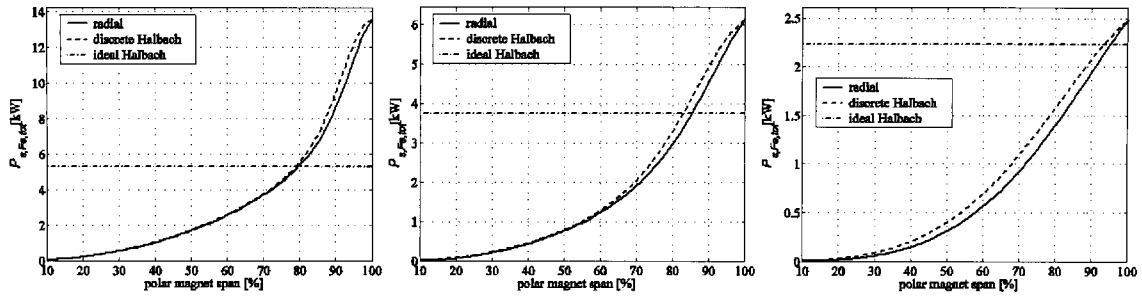

(a) $p = 1$ (b) $p = 2$ (c) $p = 4$

Fig. 8 Total stator iron loss for the first 13 space harmonics as a function of the polar magnet span and the number of pole pairs.

distributions of Fig. 5 and the radial and discrete Halbach arrays is (for the same stator current):

- 1-2-2-1: Radial: 135.7Nm; Discrete Halbach: 139.7Nm
- 1-1-2-1-1: Radial: 129.5Nm; Discrete Halbach: 133.3Nm
- 2-2-2: Radial: 137.8Nm; Discrete Halbach: 141.9Nm
- 3-3: Radial: 138.1Nm; Discrete Halbach: 142.2Nm

These results were calculated for 80% polar magnet arcs. The distribution that stands out due to its lower torque production than the others is the 1-1-2-1-1 distribution. The torque results for the other distributions show little difference.

5.2.2 Induced loss in the shielding cylinder

Concerning losses, the only loss component of interest with variation in the winding distribution is the induced loss in the shielding cylinder. The stator iron losses are not substantially influenced by the use of a different winding distribution. This is because the stator current field is neglected in its calculation (the flux density in the stator iron due to the stator currents is much lower than that due to the permanent magnets). The stator winding loss is also neglected in the optimization routines since it is very small compared to the stator iron losses.

Table 1 The induced loss in the shielding cylinder [W] for the four different winding distributions of Fig. 5 and a typical CSI current waveform. The totals are: 1-2-2-1: 79.8 W, 1-1-2-1-1: 70.1 W, 2-2-2: 90.4 W, and 3-3: 93.1 W.

	$\|n\| = 1$	3	5	1	3	5
	1-2-2-1			1-1-2-1-1		
$\|k\|=1$	0	54.95	20.23	0	50.02	18.42
3	4.319	0	0.0622	0.3152	0	0.0045
5	0.2599	0.0103	0	1.304	0.0515	0
	2-2-2			3-3		
$\|k\|=1$	0	56.65	20.86	0	56.19	20.95
3	10.45	0	0.1505	11.94	0	0.1718
5	2.222	0.0878	0	3.027	0.1196	0

Table 1 compares the induced loss in the shielding cylinder in the case of the four different winding distributions of Fig. 5. The results are listed for the fundamental, 5th and 7th space and time harmonic components. (The space harmonic number is k and its loss components are listed in the rows. The time harmonic number is n and its loss components are listed in the columns.) These calculations were done for a typical CSI current waveform. The 1-1-2-1-1 distribution shows the lowest space harmonic loss contribution, although that of the 1-2-2-1 distribution is not much higher.

5.3 Machine geometry

5.3.1 Influence of varying the machine radii on torque

In this section the machine radii defined in Fig. 6 are varied to study their effect on the electromagnetic torque production. This variation of radii results in varying the ratio R_m defined in Eq. (1).

Fig. 9 shows the fundamental space and time harmonic component of the electromagnetic torque as a function of R_m for p = 1, 2 and 4. Results for four different ratios of r_{so}/r_{mo} are presented: 0.3, 0.5, 0.735 and 0.9. R_m of the EμFER machine built by CCM is indicated by solid lines on the graphs for which r_{so}/r_{mo} = 0.735. The ratio r_{so}/r_{mo} represents the inverse of the total active air gap length between the stator and rotor surfaces, i.e., the space for the winding and permanent magnets.

Several observations may be made from Fig. 9:

- For p = 1 and p = 2, the 80/20 discrete Halbach array produces the highest torque for almost all R_m and r_{so}/r_{mo}. The exception is for small r_{so}/r_{mo} (large air gap), large R_m (thick magnets) and p > 1, where the ideal Halbach array produces higher torque.
- For a high number of pole pairs, large active air gap and thick magnets, the ideal Halbach array produces the highest torque.
- The 50/50 discrete Halbach array always produces less torque than the other three arrays, except for high p, a large air gap and thick magnets.

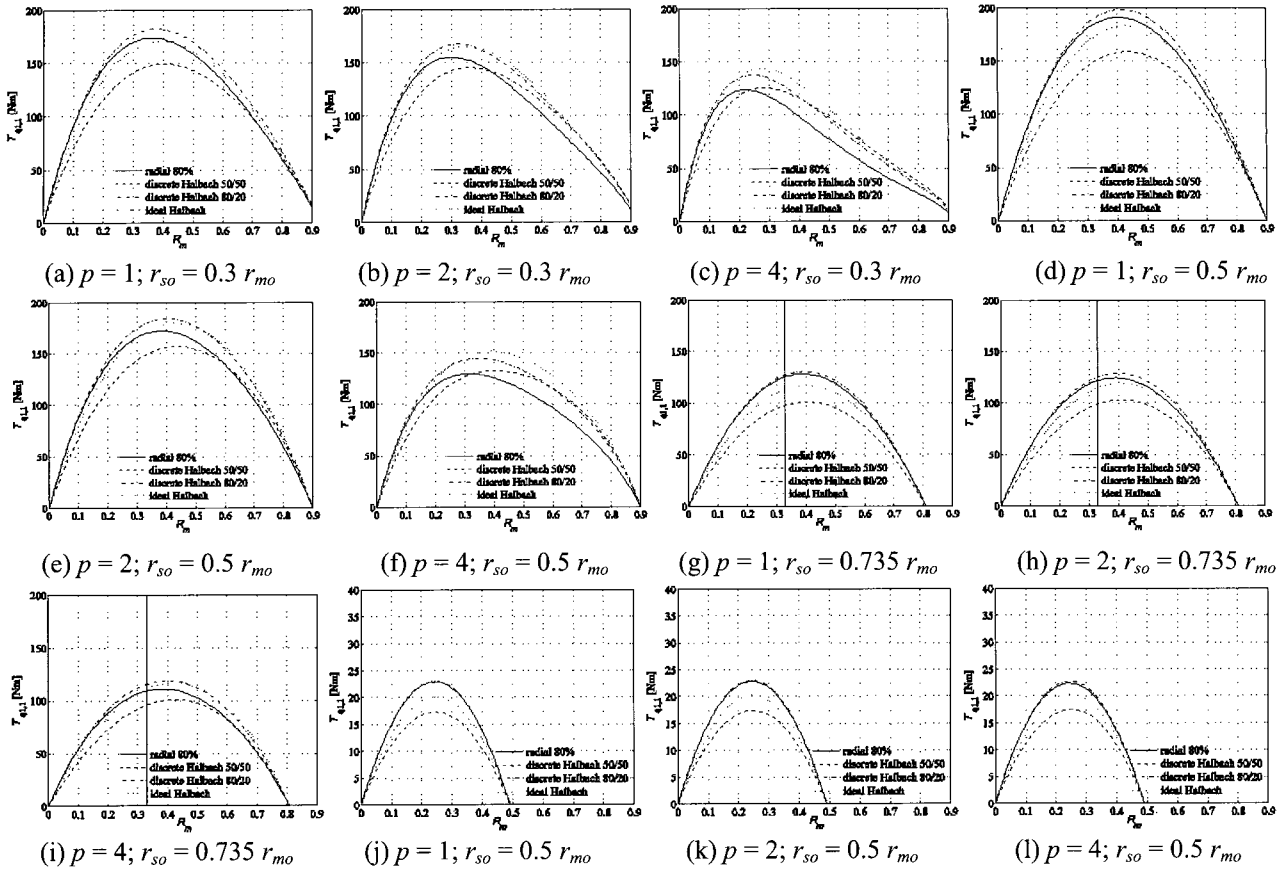

(a) $p = 1$; $r_{so} = 0.3\ r_{mo}$ (b) $p = 2$; $r_{so} = 0.3\ r_{mo}$ (c) $p = 4$; $r_{so} = 0.3\ r_{mo}$ (d) $p = 1$; $r_{so} = 0.5\ r_{mo}$

(e) $p = 2$; $r_{so} = 0.5\ r_{mo}$ (f) $p = 4$; $r_{so} = 0.5\ r_{mo}$ (g) $p = 1$; $r_{so} = 0.735\ r_{mo}$ (h) $p = 2$; $r_{so} = 0.735\ r_{mo}$

(i) $p = 4$; $r_{so} = 0.735\ r_{mo}$ (j) $p = 1$; $r_{so} = 0.5\ r_{mo}$ (k) $p = 2$; $r_{so} = 0.5\ r_{mo}$ (l) $p = 4$; $r_{so} = 0.5\ r_{mo}$

Fig. 9 Fundamental space and time harmonic of the electromagnetic torque as a function of R_m for p = 1, 2 and 4. Results for four different ratios of $r_{so}/\ r_{mo}$ are presented: 0.3, 0.5, 0.735 and 0.9. The vertical lines on (g), (h) and (i) indicate the value of R_m of the EμFER machine built by CCM.

- The radial array produces less torque in relation to the Halbach arrays when the air gap length, pole pair number and magnet thickness are increased.
- The highest torque of Fig. 9 is found in Fig. 9(d). Here, R_m is just over 0.4, the machine has one pole pair and the array is the 80/20 discrete Halbach array with two segments per pole. The torque is just under 200 Nm.
- The highest torques reached by all the arrays and pole pair numbers studied here are reached at medium air gap lengths of r_{so}/r_{mo} = 0.5 (Fig. 9(d)--(f)). For both smaller and larger active air gap lengths the torque production decreases. This decrease is drastical for very small air gaps (Fig. 9(j)--(l)).

5.3.2 Motivation of the EμFER machine's design choices

The EμFER machine constructed by CCM has a radial array with four poles, r_{so}/r_{mo} = 0.735 and R_m = 0.33; it is therefore located in Fig. 9(h) at the intersection of the R_m = 0.33-line and the radial array curve. The reason for not choosing the larger torque of Fig. 9(d) for p = 1 and the 80/20 discrete Halbach array is the high cost of rare-earth permanent magnets. An increase in active air gap length from r_{so}/r_{mo} = 0.735 to r_{so}/r_{mo} = 0.5 represents much thicker permanent magnets for the same R_m. The ratio of r_{so}/r_{mo} = 0.735 is thus preferred. Magnet cost also motivated the choice of R_m to be below that for the maximum T_e in Fig. 9(d). The difference between $T_{e,1,1}$ of one- and two-pole pair arrays is not very large once these choices have been made. Since the 80/20 discrete Halbach array's torque production is only about 2% higher than that of the radial array in Fig. 9(h) (for a 20% increase in magnet cost), the radial array is chosen.

5.3.3 Influence of varying machine radii on the stator iron losses due to the rotating permanent magnets

Graphs similar to those in Fig. 9 can be plotted for the stator iron losses due to the rotating permanent magnets. However, since there is no clear minimum in this case, these are not presented here (see [2] for these results.)

5.3.4 Influence of varying machine radii on the shielding cylinder loss due to the stator currents

As noted before, the induced eddy-current loss in the shielding cylinder is not a function of the permanent magnet array (since their relative movement is zero). This loss is,

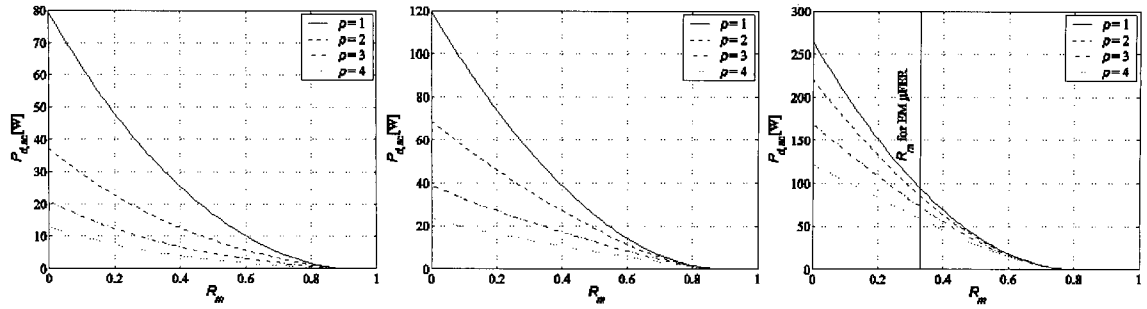

(a) $r_{so} = 0.3\ r_{mo}$ (b) $r_{so} = 0.5\ r_{mo}$ (c) $r_{so} = 0.735\ r_{mo}$

Fig. 10 Induced loss in the shielding cylinder for a typical CSI current waveform for constant J_s as a function of R_m.

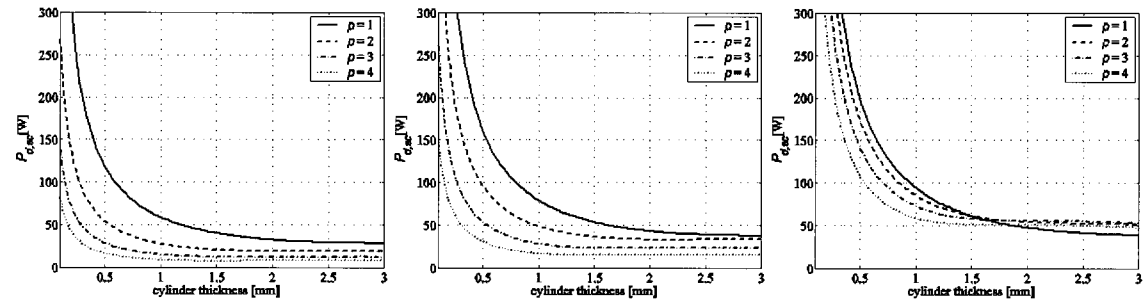

(a) $r_{so} = 0.3\ r_{mo}$ (b) $r_{so} = 0.5\ r_{mo}$ (c) $r_{so} = 0.735\ r_{mo}$

Fig. 11 Induced loss in the shielding cylinder for a typical CSI current waveform for constant J_s as a function of the cylinder thickness.

however, a function of the number of pole pairs and machine geometry (the different radii). Fig. 10 shows the induced loss in the shielding cylinder for a typical CSI current waveform for constant stator current density J_s as a function of R_m. Results are shown for three air gap lengths: r_{so}/r_{mo} = 0.3, 0.5 and 0.735. The solid line in Fig. 10(c) indicates R_m for the EµFER machine. It can be clearly seen that the loss increases as the distance between the shielding cylinder and the stator currents decreases. The difference between the pole pair numbers is once again due to more leakage for higher p.

5.3.5 Shielding cylinder loss as a function of the cylinder thickness

In Fig. 11, the value for R_m has already been chosen, and the effect of varying the cylinder thickness on the induced loss is studied. (The cylinder thickness in Fig. 10 is 1 mm.)

It can be seen that the losses reduce with cylinder thickness. However, a trade-off solution has to be found between low loss and the mechanical difficulty of weight containment of a thicker shielding cylinder. In Fig. 11(c) it can be seen that the shielding cylinder loss does not significantly decrease when the cylinder thickness is increased from 1 mm to 2 mm; 1 mm is therefore the chosen thickness.

6. Conclusion

In this paper, optimization of a flywheel PMSM with an external rotor and a slotless stator was discussed. Three optimization criteria were chosen: (1) torque; (2) total stator losses and (3) induced eddy current loss on the rotor. The influence of the permanent-magnet array, winding distribution and machine geometry on these criteria was investigated. The paper showed that an analytical model of the machine greatly aids in optimization studies. The optimization results combined with engineering judgment lead to the design of the EµFER machine built for the hybrid electric city bus. The absolute optimum could not be used due to high magnet cost, but a good trade-off solution was found.

Acknowledgment

The authors would like to thank the Centre for Construction in Mechatronics (CCM) B.V. of Nuenen, the Netherlands, the industrial partner in this project.

References

[1] W. D. Jones, "Hybrids to the rescue", in *IEEE Spectrum*, January 2003.

[2] S. R. Holm, "Modelling and Optimization of a Permanent-Magnet Machine in a Flywheel", Ph.D. dissertation, Delft University of Technology, Delft, the Netherlands, November 2003.

[3] G. Genta, *Kinetic Energy Storage – Theory and practice of advanced flywheel systems.* London: Butterworths, 1985, ISBN 0-408-01396-6.

[4] F. J. M. Thoolen, "Development of an Advanced High Speed Flywheel Energy Storage System", Ph.D. dissertation, Eindhoven University of Technology, Eindhoven, the Netherlands, December 1993.

[5] A. Arkadan, R. Vyas, J.Vaidya, and M. Sha, "Effect of Toothless Stator Design on Core and Stator Conductors Eddy Current Losses in Permanent Magnet Generators", in *IEEE Transactions on Energy Conversion*, vol. 7, no. 1, March 1992.

[6] J. van der Veen, L. Offringa, and A. Vandenput, "Minimizing rotor losses in high-speed high-power permanent magnet synchronous generators with rectifier load", in *IEE Proc.-Electr. Power Appl.*, vol. 144, no. 5, September 1997, pp. 331-337.

[7] S. A. Sharkh, M. Harris, and N. T. Irenji, "Calculation of rotor eddy-current loss in high-speed PM alternators", in *Conference Record, International Conference on Electrical Machines and Drives (EMD 1997)*, 1997, pp. 170-174.

[8] F. Deng, "Commutation-Caused Eddy-Current Losses in Permanent-Magnet Brushless DC Motors", in *IEEE Transactions on Magnetics*, vol. 33, no. 5, September 1997, pp. 4310-4318.

[9] F. Deng and T. W. Nehl, "Analytical Modelling of Eddy-Current Losses Caused by Pulse-Width Modulation Switching in Permanent-Magnet Brushless Direct-Current Motors", in *IEEE Transactions on Magnetics*, vol. 34, no. 5, September 1998, pp. 3728-3736.

[10] H. Polinder, "On the losses in a high-speed permanent magnet generator with rectifier", Ph.D. dissertation, Delft University of Technology, June 1998.

[11] Z. Q. Zhu, K. Ng, N. Schofield, and D. Howe, "Analytical Prediction of Rotor Eddy Current Loss in Brushless Machines Equipped with Surface-Mounted Permanent Magnets, Part II: Accounting for Eddy Current Reaction Field", in Proceedings of the Fifth International Conference on Electrical Machines and Systems (ICEMS 2001), vol. 2, no. 5, September 2001, pp. 810-813.

[12] K. Halbach, "Design of Permanent Multipole Magnets with Oriented Rara Earth Cobalt Material", in Nuclear Instruments and Methods, vol. 169, Berkerley, USA, 1980, pp. 1-10.

[13] K. Atallah, D. Howe, and P. H. Mellor, "Design and Analysis of Multi-Pole Halbach (Self-Shielding) Cylinder Brushless Permanent Magnet Machines", in Eighth International Conference on Electrical Machines and Drives, no. 444, London, UK, 1997, pp. 376-380.

Robert Holm

He was born in Johannesburg, South Africa, in 1973. He received the B.Eng. (1996) and M.Eng. (1998) degrees in electrical engineering and the B.Sc.(Hons) degree in applied mathematics (1998) from the Rand Afrikaans University, Johannesburg, South Africa, and the Ph.D. degree in electrical engineering (2003) from the Delft University of Technology, the Netherlands. From 1998 - 1999 he worked in industry as a power electronics design engineer, and from 1999 - 2003 he worked as a Ph.D. researcher at the Delft University of Technology. Since 2004 he is senior lecturer at the University of Johannesburg (formerly Rand Afrikaans University). His current research interests include permanent-magnet machines, electromagnetics and energy storage technologies.

Henk Polinder

He holds a M.Sc. degree (1992) and a Ph.D. degree (1998) in electrical engineering from Delft University of Technology, the Netherlands. From 1996 to 2003, he was an assistant professor, and since 2003, he has been an associate professor at Delft University of Technology in the field of electrical machines and drives. In 1998 and 1999, he was part-time detached at the wind turbine manufacturer Lagerwey to design a direct-drive generator. In 2001, he was part-time detached at Philips CFT. In July and August 2002, he was a visiting scholar at the University of Newcastle-upon-Tyne. He is author and co-author of over 50 papers. His main research interests are design aspects of electrical machines for renewable energy and mechatronic applications.

Braham Ferreira

He received the B.Sc.Eng., M.Sc..Eng., and Ph.D. degrees in Electrical Engineering from the Rand Afrikaans University, Johannesburg, South Africa in 1981, 1983 and 1988 respectively.

In 1981 he was with the Institute of Power Electronics and Electric Drives, Technical University of Aachen, and worked in industry at ESD (Pty) Ltd from 1982-1985. From 1986 until 1997 he was at the Faculty of Engineering, Rand Afrikaans University, where he held the Carl and Emily Fuchs Chair of Power Electronics in later years. Since 1998 he is a professor at the Delft University of Technology in The Netherlands.

Dr. Ferreira is a fellow of the IEEE. During 1993-4 he was chairman of the South African Section of the IEEE. He was the founding chairman of the IEEE Joint IAS/PELS Benelux chapter in 1999. He served as the transactions review chairman of the IEEE IAS Power Electronic Devices and Components Committee during 1999-2003 and is an associate editor of the PELS Transactions. He is a member of the IEEE PESC Adcom is since 2005 the treasurer of the IEEE PELS. Dr. Ferreira served as chairman of the CIGRE SC14 national committee of the Netherlands and was a member of the executive committee of the EPE Society.